World Scientific
www.worldscientific.com

JAPAN SOCIETY OF CIVIL ENGINEERS
COASTAL ENGINEERING COMMITTEE

Coastal Engineering Journal, Vol. 52, No. 3 (2010) 215–234

DOI: 10.1142/S057856341000218X

A NUMERICAL SIMULATION OF A TIDAL BORE FLOW

SHO-ICHI FURUYAMA
Department of Electronics and Computer Engineering,
Toyama National College of Technology,
1-2 Ebie-Neriya, Imizu, Toyama 933-0293, Japan
shoichi@nc-toyama.ac.jp
http://www.toyama-cmt.ac.jp/∼shoichi/

HUBERT CHANSON
School of Civil Engineering,
The University of Queensland,
Brisbane QLD 4072, Australia
h.chanson@uq.edu.au
http://www.uq.edu.au/∼e2hchans/

Received 10 December 2008
Revised 5 July 2010

A numerical model was developed based on the Cubic-Interpolated Pseudo-particle (CIP) Combined Unified Procedure (CIP-CUP or C-CUP) method equipped with a Large Eddy Simulation (LES) model and a re-initialization method. The model was validated and applied to the tidal bore flow with a weak breaking front. In the tidal bore flow, the model equipped with a LES turbulence model reproduced accurately the large deformation of the free surface during the bore formation by rapid closure of a downstream gate. The free-surface profile and surge front celerity data were in good agreement with the experimental data of [Koch and Chanson 2009, J. Hyd. Res. IAHR]. At a fixed sampling location, the numerical results showed the existence of some short-lived flow reversal next to the bed immediately after the bore front passage. This flow feature was documented by [Koch and Chanson 2009] and [Chanson 2009, Eur. J. Mech. B. Fluids].

Keywords: Tidal bores; turbulence; surges; numerical method; rapidly-varied free-surface flow; Cubic-Interpolated Pseudo-particle (CIP); CIP Combined Unified Procedure (C-CUP); Large Eddy Simulation (LES).

1. Introduction

A number of hydraulic engineering applications cannot be solved analytically because of the complexity of the relevant equations. One example is the tidal bore flow.

The application is unsteady open channel flows characterized by a rapidly changing free-surface.

In macro-tidal estuaries, a tidal bore may form during spring tide conditions when the flood tide is confined to a narrow funneled channel. The bore is a series of waves propagating upstream as the tidal flow turns to rising. The most powerful tidal bores are probably those of the Qiantang river (China) and the "pororoca" of the Amazon river (Brazil). Smaller tidal bores occur on the Severn river near Gloucester, England, on the Garonne and Dordogne rivers, France, at Turnagain Arm and Knik Arm, Cook Inlet (Alaska), in the Bay of Fundy (at Petitcodiac and Truro), on the Styx and Daly rivers (Australia), and at Batang Lupar (Malaysia). At the coast of Japan, Tsunami-induced bore which is a kind of tidal bore, was observed in the major earthquake; e.g. Shuto [1985]. Figure 1 illustrates tidal bores in the Baie du Mont Saint Michel and Garonne River. The occurrence of tidal bores has a significant impact on river mouths and estuarine systems; e.g. Chanson [2007, 2009]. Bed erosion and scour take place beneath the bore front while suspended matters are carried upwards in the ensuing wave motion. The process contributes to significant sediment transport with deposition in upstream intertidal areas. The existence of tidal bores is based upon a fragile hydrodynamic balance, which may be easily disturbed by changes in boundary conditions and freshwater inflow; e.g. Malandain [1988]. Man-made interventions led to the disappearance of several bores with often adverse impacts on the ecosystem: e.g. the mascaret of the Seine river (Fra.) no longer exists and the Colorado river bore (Mex.) is drastically smaller after dredging. Although the fluvial traffic gained in safety in each case, the ecology of estuarine zones were adversely affected. The tidal bores of the Couesnon (Fra.) and Petitcodiac (Ca.) rivers almost disappeared after construction of an upstream barrage. At Petitcodiac, this yielded the elimination of several diadromous fish species, including the American shad, Atlantic salmon, Atlantic tomcod, Striped bass and Sturgeon; e.g. Locke *et al.* [2003].

There are numerous visual accounts of tidal bores, and most occurrences showed well-defined undulations behind the leading wave, that is an undular bore process. The other type of bores is the breaking bore. Field measurements in tidal bores are very limited and most studies recorded a limited number of parameters with relatively coarse resolutions in terms of time scales, spatial resolutions and velocity magnitudes. Further all field studies were fixed-point measurements, but a tidal bore is a very dynamic process which extends over several kilometers, sometimes tens of kilometers. The bore shape and characteristics evolve rapidly with time in response to change in bathymetry. Previous studies rarely encompassed turbulence except in a few limited studies; e.g. Hornung *et al.* [1995]; Koch and Chanson [2009].

Some numerical simulations were applied to the bore problem. Hirt and Nichols [1981] applied the VOF method to reproduce the bore, but the numerical results

(a)

(b)

Fig. 1. Photographs of tidal bores. (a) Tidal bore in the Baie du Mont Saint Michel (France) viewed from Pointe du Grouin du Sud on 14 October 2008 — Bore propagation from right to left. (b) Tidal bore of the Garonne River at Podensac (France) on 28 Sept 2008 — Looking at the incoming bore.

were simply tested in terms of the free-surface elevation. Madsen *et al.* [2005] applied their models to a case study of the tidal bore in Huangzhou Bay and Qiantang River. Their models involved the upwind treatment of convective terms, the central differences combined with the dissipative interface, the forward time-centering and the various combinations of these techniques. The model results were shown to be in good agreement with field data.

This paper describes a numerical simulation method Toyama CoAstal flow Simulator (TCAS) and the results for the free-surface flow of tidal bore. The TCAS includes the Cubic Interpolation Pseudo-particle (CIP) method, CIP Combined Unified Procedure (CIP-CUP or C-CUP) method for the base numerical method and equips the LES for the turbulence model. By definition, the fluid is compressible fluid and the Poisson equation for pressure is derived in TCAS. The equation is solved in terms of the local sound velocity in each phase (i.e. gas and liquid phases). The method has the ability to be solved using an unified procedure even if the phases are different. Though the method solves the interaction between the gas and the liquid, the complex boundary conditions are not necessary at the free surface; e.g. Yabe *et al.* [2005]. It is believed that the C-CUP method is a reasonable choice for the free surface flow modeling in many civil engineering applications. There are some previous studies which applied the C-CUP method to civil engineering applications. Mizutani *et al.* [2002] developed a numerical scheme to solve gas and liquid mixing flow-field based C-CUP method. They applied the scheme to the dam break problem. They improved the numerical diffusion at the air-water interface by using a complete conservation algorithm. Yokoi and Xiao [2002] used the C-CUP method for analyzing the circular hydraulic jumps with a Continuum Surface Force (CSF) model. Momoki and Yoneyama [2005] used the C-CUP method to calculate the impulsive breaking wave force that acts on coastal structures with the conservative CIP method, i.e. Conservative Semi-Lagrangian (CSL) method; e.g. Nakamura *et al.* [2001]. Hong *et al.* [2005] tested the C-CUP method with the level-set method in the dam breaking problem and applied it to analyze the breaking phenomena of ships' waves in narrow and shallow waterways. Kawasaki [2005a,b]; Kawasaki and Hakamata [2006] developed DOLPHIN-2D/3D numerical model based on the CIP method with LES turbulence model and they solve the solid-gas-liquid interactions.

In this paper, Sec. 2 details with the numerical method. In the section, the C-CUP method and additional techniques for the stable calculation are described. Numerical results are presented in Sec. 3, and they are discussed in Sec. 4. The model simulates the flow field of the tidal bore flow with weak breaking flow. It is compared with experimental data by Koch and Chanson [2009] and Chanson [2009].

The TCAS program code (TCAS20080104A.c) in this study is available to download from "`http://www.toyama-cmt.ac.jp/~shoichi/TCAS/`".

2. Methodology

2.1. *Governing equations*

The two-dimensional momentum and pressure equations coupling with the filtered equations for the Large Eddy Simulation (LES) modeling; e.g. Lesieur *et al.* [2005]:

$$\frac{\partial \rho}{\partial t} + \bar{u}_j \frac{\partial \rho}{\partial x_j} = -\rho \frac{\partial \bar{u}_i}{\partial xi} \tag{1}$$

$$\frac{\partial \bar{u}_i}{\partial t} + \bar{u}_j \frac{\partial \bar{u}_i}{\partial x_j} = -\frac{1}{\rho}\frac{\partial \bar{P}}{\partial x_i} + \frac{\partial}{\partial x_i} + (2(\nu + \nu_e)\bar{D}_{ij})) - g\delta_{i2} \tag{2}$$

$$\frac{\partial \bar{P}}{\partial t} + u_i \frac{\partial \bar{P}}{\partial x_i} = -\rho C_s^2 \frac{\partial \bar{u}_i}{\partial x_i} \tag{3}$$

$$\bar{D}_{ij} = \frac{1}{2}\left(\frac{\partial \bar{u}_i}{\partial x_j} + \frac{\partial \bar{u}_j}{\partial x_i}\right) \tag{4}$$

where i, $j = 1$ and 2 correspond to the coordinates x and y respectively. Here u_i ($i = 1$ and 2) are the velocity components in the x and y directions, ρ is the density, t is the time, ν is the kinematic viscosity, g is the gravitational acceleration constant, δ_{ij} is the Kronecker delta, C_s is the local sound velocity $\bar{u}_i$ means the Grid Scale (GS) value of the velocity component u_i, ν_e is the Sub Grid Scale (SGS) eddy viscosity, $\bar{D}_{ij}$ represents the strain-rate tensor and $\bar{P}$ is defined as:

$$\bar{P} = \bar{p} + \frac{1}{3}\rho\tau_{ii} \tag{5}$$

where $\tau_{ij} = \bar{u}_i\bar{u}_j - \bar{u}_i\bar{u}_j$ is called the residual stress. The $\bar{p}$ value is deduced from the modelling of the stress. In this study, $\bar{P}$ is calculated coupling with Eqs. (2) and (3) (i.e. $\bar{p}$ is not calculated). The method applies the Smagorinsky model, i.e. Smagorinsky [1963], for the SGS eddy viscosity coefficient ν_e:

$$\nu_e = (C_{\mathrm{smg}}\Delta)^2|\bar{D}| \tag{6}$$

where Δ is the filter width (i.e. the grid size in this case) and C_{smg} is the Smagorinsky constant. In general $C_{\mathrm{smg}} = 0.10 \sim 0.15$ is used for the turbulent shear flows. $|\bar{D}|$ means the absolute value of the strain-rate tensor on GS:

$$|\bar{D}| = \sqrt{2\bar{D}_{ij}\,\bar{D}_{ij}} \tag{7}$$

where the strain-rate tensor on the grid point (i.e. $\bar{D}_{ij}$) was defined in Eq. (4).

2.2. *C-CUP method*

Yabe *et al.* [1991] proposed the Cubic-Interpolated Pseudo-particle (CIP) method. In the method, each grid point has the gradient information of the physical values,

as well as the interpolated values between a grid and the neighbor grid. Hence, the CIP has an ability to solve the advection phase with high accuracy and stability.

A notable feature of CIP method is to split the governing equations to the advection phase and the non-advection phase, and then the method solves each phase equation independently. In the case of Eqs. (1) to (3), these equations are split as:

$$\frac{\partial \rho}{\partial t} + \bar{u}_j \frac{\partial \rho}{\partial x_j} = 0 \quad \text{(Advection phase for density)} \tag{8}$$

$$\frac{\partial \rho}{\partial t} = -\rho \frac{\partial \bar{u}_i}{\partial x_i} \quad \text{(Non-advection phase for density)} \tag{9}$$

$$\frac{\partial \bar{u}_i}{\partial t} + \bar{u}_j \frac{\partial \bar{u}_i}{\partial x_j} = 0 \quad \text{(Advection phase for velocity)} \tag{10}$$

$$\frac{\partial \bar{u}_i}{\partial t} = -\frac{1}{\rho} \frac{\partial \bar{P}}{\partial x_i} \quad \text{(Non-advection phase for velocity: pressure term)} \tag{11}$$

$$\frac{\partial \bar{u}_i}{\partial t} = \frac{\partial}{\partial x_i}(2(\nu + \nu_e)\bar{D}_{ij})) - g\delta_{i2} \quad \text{(Non-advection phase for velocity: diffusion and gravity term)} \tag{12}$$

$$\frac{\partial \bar{P}}{\partial t} + u_i \frac{\partial \bar{P}}{\partial x_i} = 0 \quad \text{(Advection phase for pressure)} \tag{13}$$

$$\frac{\partial \bar{P}}{\partial t} = -\rho C_s^2 \frac{\partial \bar{u}_i}{\partial x_i} \quad \text{(Non-advection phase for pressure)} \tag{14}$$

The CIP method is coupled with the unified procedure for the flow field calculation of the two or more phases. It is called the CIP-Combined Unified Procedure (CIP-CUP or C-CUP) method. The method introduces a time dependent Poisson equation for pressure. By definition of the sound speed in both gas and liquid phases, the method solves the Poisson equation. Combining Eqs. (11) and (14), $\bar{P}$ is solved by the following Poisson equation:

$$\nabla \cdot \left(\frac{\nabla \bar{P}^{**}}{\rho^n} \right) = \frac{\bar{P}^{**} - \bar{P}^n}{\rho^n C_s^2 \Delta t} + \frac{1}{\Delta t} \nabla \cdot \mathbf{u}^n \tag{15}$$

where the superscript n is a current time step and the superscript ** is the time step after the pressure calculation (i.e. $\bar{P}^{**}$ is the iteration solution after the pressure calculation and $\bar{P}^n$ is the known pressure value at the time n), $\mathbf{u} = (u_1, u_2)$ and C_s is the means sound celerity that is function of the physical properties (e.g. liquid or gas phase). That is, a function of physical conditions is needed. The following shape

function is a popular way to estimate the physical conditions:

$$\frac{\partial \phi}{\partial t} + \bar{u}_j \frac{\partial \phi}{\partial x_j} = 0 \tag{16}$$

where ϕ represents the physical property (i.e. air or water) and defined at each grid points (l, m) as follows:

$$\begin{cases} \phi_{l,m} = 0 & \text{for air} \\ \phi_{l,m} = 1 & \text{for water} \end{cases} \tag{17}$$

In other words, ϕ is the local and instantaneous liquid fraction. Equation (16) is an advection equation. The CIP method solves the advection equation in high accuracy.

Eddington [1970] studied the sound velocity in a two-phase (liquid-gas) tunnel. He showed the isothermal speed of sound in an air-water mixture as a function of the gas-to-liquid volume ratio. In his study, a minimum sound speed is 19.8 m/s (65 fps) at the gas-to-liquid volume ratio of 1.0, and the sound speed has a non-linear relation with the gas-to-liquid volume ratio. Shimizu *et al.* [2001] simplify the character of the sound speed as follows:

$$C_s^2 = (1 - \phi) C_{s,\text{air}}^2 + \phi C_{s,\text{water}}^2 \tag{18}$$

where $C_{s,\text{air}}$ and $C_{s,\text{water}}$ are estimated as:

$$C_{s,\text{air}} = \sqrt{\gamma \frac{\bar{P}}{\rho_{\text{air}}}} \tag{19}$$

$$C_{s,\text{water}} = \sqrt{\kappa \frac{\bar{P} + B}{\rho_{\text{water}}}} \tag{20}$$

where γ is the specific heat rate, $\bar{P}$ is the pressure, ρ_{air} is the air density and ρ_{water} is the water density. Here κ and B are experimental coefficients equal respectively to 7.15 and 304.9 M Pa. In this study, the speed of sound is calculated by a similar method. Equation (15) is solved by the Successive Over Relaxation (SOR) method and the staggered grid is used to prevent the pressure oscillation; e.g. Kajishima [2003].

Equations (8)–(14) and (16) are expressed by the time differential expression. Here the n and $n+1$ mean a time step. The $n+1$ is the time step after the Δt from the time step n. The C-CUP method needs a 3-step calculation for Δt integration, i.e.

(1) the pressure calculation,
(2) the non-advection phase calculation,
(3) the advection phase calculation.

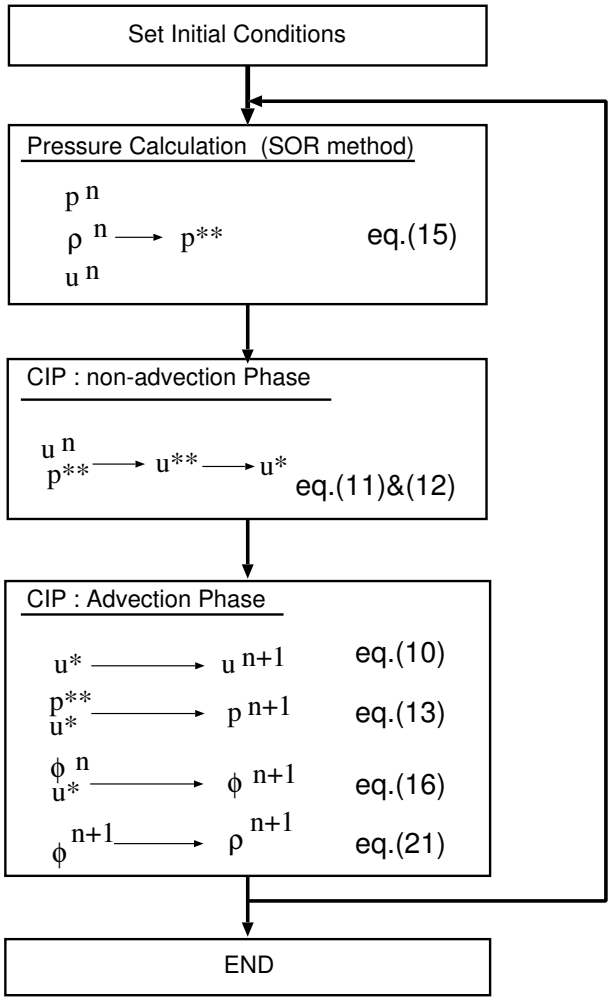

Fig. 2. Flowchart of all model in this study.

The time step after the pressure calculation is denoted as ** and * after the non-advection phase calculation. The superscripts are used in Fig. 2. In these equations and the figure, $\overline{p^{**}}$ means the value after the pressure calculation (e.g. the box of Pressure Calculation) and the $\overline{u^{**}}$ means the value after the non-advection phase calculation using the pressure value ($\overline{p^{**}}$) (e.g. the box of CIP: non-advection phase in Fig. 2).

2.3. *Stability and conservation techniques*

Some technical methods were added to the original C-CUP method for stable and conservative calculations. The density values are only the water density and the air density under the theoretical condition in this simulation. In the numerical study, some grid points may have intermediate values. Because the CIP method implies

the calculation of the advection equation at high order, the density was calculated by using the shape function value as follows:

$$\rho = \phi\rho_{\text{water}} + (1-\phi)\rho_{\text{air}} \tag{21}$$

The order of Δt is restricted by the sound speed (about $10^{-5} \sim 10^{-4}$ s). In many civil engineering applications, a huge number of time steps is required. With such long integration times, numerical errors (i.e. numerical diffusion error) influence the calculation results. A re-initialization method is generally used; e.g. Yokoi and Xiao [2002]; Hong *et al.* [2005]; Mizutani *et al.* [2002]. This method defines a gas region ($\phi = 0$), and liquid region ($\phi = 1$), and a surface region ($\phi = 0.5$). First the grid points including $\phi = 0.5$ are found and the number of grid points are counted (N_{surface}). At the other points, the following conditions are applied,

$$\begin{cases} \phi = 0 & \text{if } \phi < 0.5 \\ \phi = 1 & \text{if } \phi > 0.5 \end{cases} \tag{22}$$

Figure 3 shows a schematic of the re-initialization method. There is the numerical diffusion area with grid points across the free-surface, before applying the re-initialization method, i.e. Fig. 3 (left). The re-initialization method keeps the numerical diffusion area within 1 grid points using Eq. (22) as shown in Fig. 3 (right).

The amount of differential (AD) value in the whole simulated region between the re-initialized $\phi_{l,m}^{\text{rini}}$ value and the original $\phi_{l,m}^{\text{orig}}$ value is calculated as:

$$AD = \Sigma_{l,m}(\phi_{l,m}^{\text{orig}} - \phi_{l,m}^{\text{rini}}) \tag{23}$$

Most of AD value comes from the grid points of the contact surface region, i.e. the numerical diffusion area in Fig. 3 (left). It is the effect of the numerical diffusion

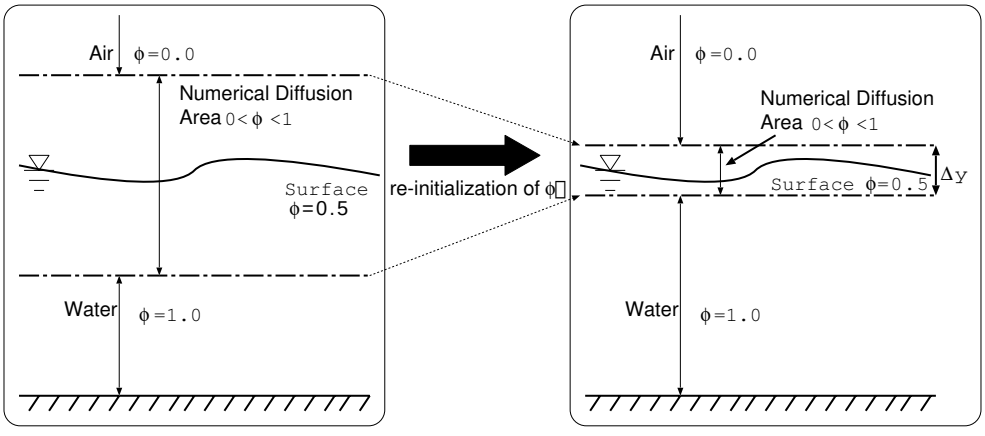

Fig. 3. Re-initialization method: before applying the method (left) and after applying the method (right).

at the discontinuity contact surface of ϕ (water-air contact region). The value that divided AD by a number of the contact surface grid (i.e. N_{surface}) is calculated as:

$$\frac{AD}{N_{\text{surface}}} \tag{24}$$

and the value is added to ϕ at the contact surface grid points [i.e. the numerical diffusion area in Fig. 3 (right)]. This technique induces a stable calculation for the shape function for ϕ, hence for ρ. The C-CUP method is not a conservative technique, but the method satisfied the conservative law using the re-initialization method.

3. Results

Koch and Chanson [2009] studied the turbulence in tidal bores and positive surges. Their experimental data was used for the validation of the numerical model.

Figure 4 presents the initial flow field conditions and the dimensions of the calculation domain. The initial steady flow motion (depth = d_0) is from the channel right to the left with an initially steady velocity V_0 at $t < 0.0$ s. At $t = 0.0$ s the gate is partially shut, with a gate opening after closure of $h = 0.0125$ m. Table 1 shows the details of the calculations. The grid size (Δx and Δy) is 0.0125 m and Δt is set to 1.0×10^{-4} s. The number of grids is 12,600 in the study. The boundary conditions at the right wall are the upstream flow conditions. The initial water depth is $d_0 = 0.0875$ m and the initial velocity is 1.0 m/s. The velocity of the inlet air flow is 1.0 m/s above the water. The velocities of the water and the air at the right side of the calculated domain are maintained while calculation is at the boundary condition. In this study, the non-slip condition is applied to the walls and the bottom bed because of the TCAS aims to solve the velocity profiles in the

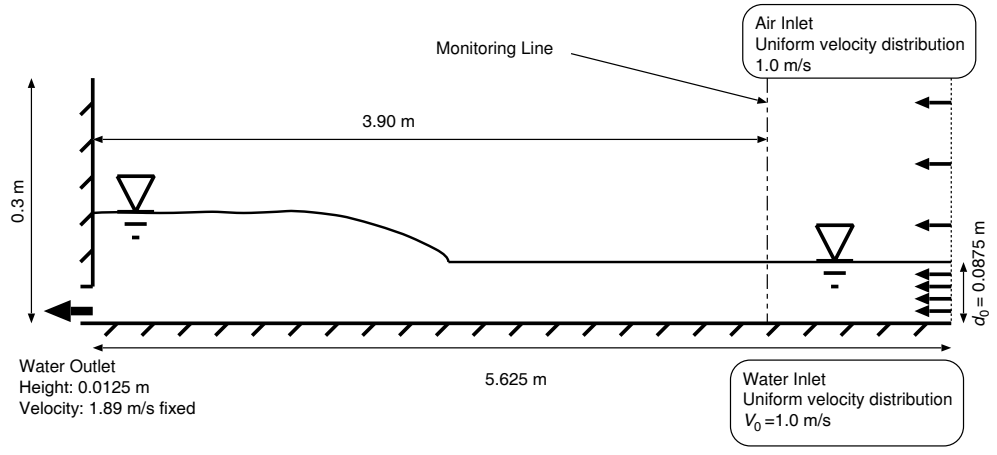

Fig. 4. Initial condition and geometries: the initial steady flow motion (depth = d_0) is from the channel right to the left with an initially steady velocity V_0 at $t < 0.0$ s. At $t = 0.0$ s the gate is partially shut, with a gate opening after closure of $h = 0.0125$ m.

Table 1. Parameter specifications.

Parameters	
Δx, Δy	0.0125 m
Δt	1.0×10^{-4} s
Num. of grids	12,600 ($= 450 \times 28$)
Size of calculation area (*Length* $\times$ *Height*)	9.6 m $\times$ 0.3 m
Inlet height (d_0)	0.0875 m
Inlet velocity	1.0 m/s
Outlet height (h)	0.0125 m
Outlet velocity	1.89 m/s fixed
Residual for SOR and Num. of Max. iterations	10^{-12}, 10,000 *times*
Specific heat rate	1.4
Water viscosity μ_{water}	1.002×10^{-3} Pa $\cdot$ s
Air viscosity μ_{air}	1.82×10^{-5} Pa $\cdot$ s
Water density ρ_{water}	998.2 kg/m^3
Air density ρ_{air}	1.166 kg/m^3
Gravitational acc. coef. g	9.8 m/s^2
Smagorinsky coefficient C_{smg}	0.1
Monitoring line	$x = 3.9$ m
	from the gate (i.e. left wall)

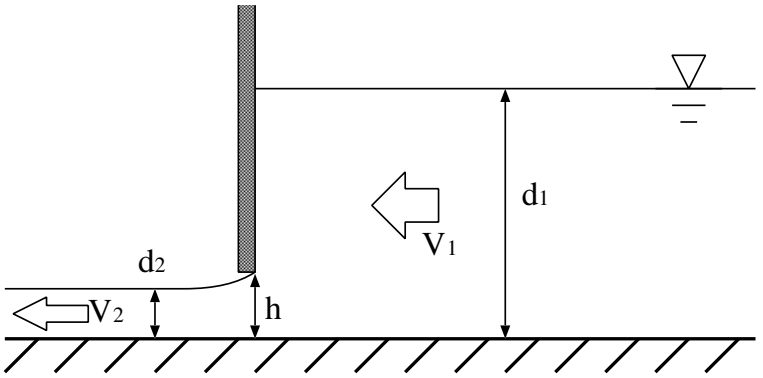

Fig. 5. Evaluation of the outlet velocity: d_1 and V_1 is the depth and the mean velocity of the right side of the gate, and d_2 and V_2 is the depth and the mean velocity of the left side of the gate.

viscous sublayer; e.g. Kajishima [2003]. The wall function is neglected for the simple boundary condition, but the discussion of the condition is for future works. The discharge velocity is estimated by the integral form of the Bernoulli equation,

$$d_1 + \frac{V_1^2}{2g} = d_2 + \frac{V_2^2}{2g} \tag{25}$$

where d_1 and V_1 is the depth and the mean velocity of the right side of the gate, and d_2 and V_2 is the depth and the mean velocity of the left side of the gate (Fig. 5). The

equation is valid for the no-energy loss condition, but the energy loss is assumed to be small enough in the study. In the studies of Koch and Chanson [2009], $d_1 = 0.18$ m, $V_1 = 0.13$ m/s, $d_2 = 0.012$ m and $V_2 \approx 1.89$ m/s. d_2 is about 60% of the gate opening height (h) as observed by Koch and Chanson [2009]. In the TCAS, the outlet condition is defined as the boundary condition. The outlet height is defined as 0.0125 m which is lower than the gate opening height ($h = 0.02$ m) by the studies of Koch and Chanson [2009], and the outlet velocity condition is fixed in the calculation. The bottom bed is fixed and the no-slip condition applied. The open boundary condition is applied to the top of the calculation domain. The convergence for the pressure calculation is set at 10^{-12}, and the iteration process is stopped at 10,000 times if convergence is not achieved (i.e. max. iterations). The turbulence parameter (i.e. Smagorinsky parameter) is set to 0.1.

The sampling locations are set at $x = 3.9$ m from the left wall. Figure 6 illustrates the data sampling points of u (black triangles) and v (light gray triangles).

The definition points of u and v are different, because the staggered grids are used in TCAS. A set of sampling point of u and v is expressed in Layers as shown in

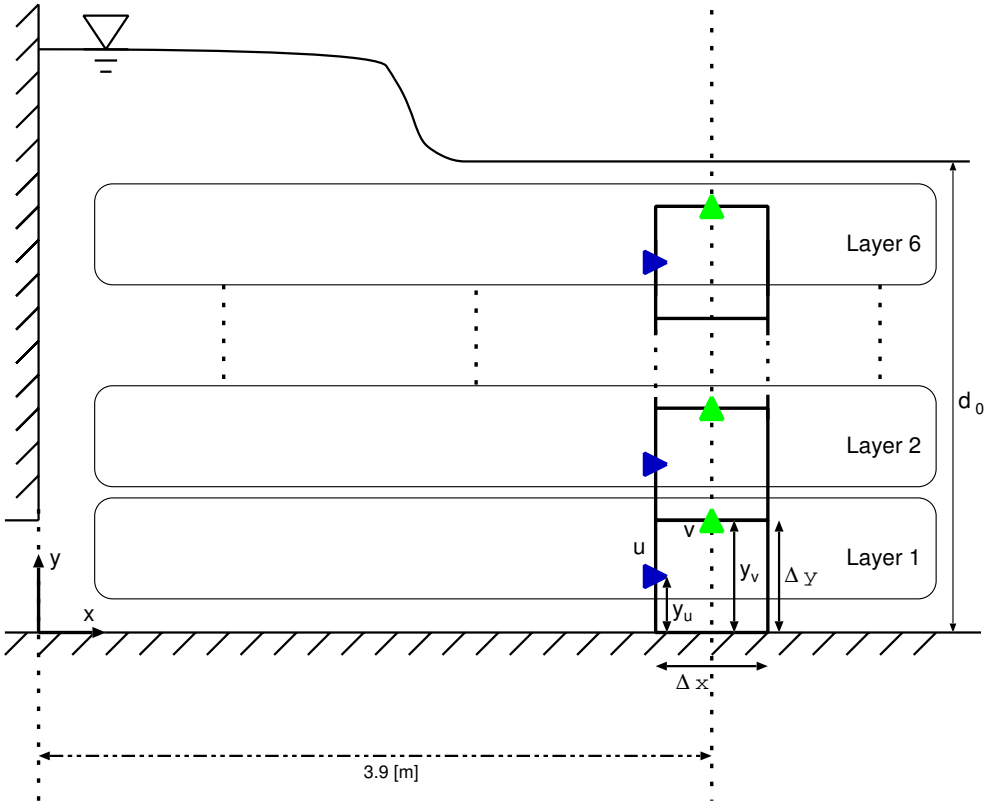

Fig. 6. Sampling layer: the sampling locations are set at $x = 3.9$ m from the left wall. The definition points of u and v are different, because of the staggered grids are used in TCAS. A bottom layer is defined as Layer 1, and the top layer is defined as Layer 6.

Fig. 6. A bottom layer is defined as Layer 1, and the top layer is defined as Layer 6. In Table 2, the height of the layer and the ratio of the layer and the d_0 are shown.

Figure 7 illustrates the generation of a weak positive surge by a rapid partial gate closure for $t = 0.0$ to 0.42 s. The black and the white region shows the water and the air respectively.

Figure 8 illustrates the propagation of a weak positive surge by a rapid partial gate closure from $t = 1.0$ to 9.0 s. The black and the white region shows the water and the air respectively.

Figure 9 shows the pressure profiles for vertical direction at $x = 0.0$ (solid-line), 0.2 (broken-line), 3.9 (dotted-line), 5.0 (dashed-line) m at $t = 7.0$ s. The horizontal axis is pressure Pa and the vertical axis is the height from the bed.

Figure 10 shows the velocity profile at the positive surge at $t = 7.0$ s. The length of the vectors represent the speed of the flow. The black and white regions show the water and the air respectively.

Figure 11 shows dimensionless instantaneous water depth d/d_0 (dotted-line) and velocity components V_x/V_* (black line), V_y/V_* (light-gray line) as functions of the

Table 2. Layer specification at the sampling locations. y_u and y_v is the sampling height from the bottom bed for u and v respectively. y_u/d_0 and y_v/d_0 is the ratio of the sampling height and d_0.

Layer	Position of u: y_u m	y_u/d_0	Position of v: y_v m	y_v/d_0
1	0.00625	0.071429	0.01250	0.142857
2	0.01875	0.214286	0.02500	0.285714
3	0.03125	0.357143	0.03750	0.428571
4	0.04375	0.500000	0.05000	0.571429
5	0.05625	0.642857	0.06250	0.714286
6	0.06875	0.785714	0.07500	0.857143

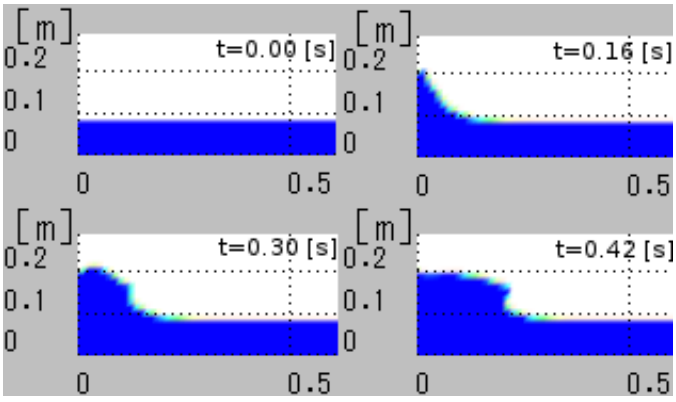

Fig. 7. Initial free-surface flow around the left wall: $t = 0.00$ s (left top), $t = 0.16$ s (right top), $t = 0.30$ s (left bottom) and $t = 0.42$ s (right bottom).

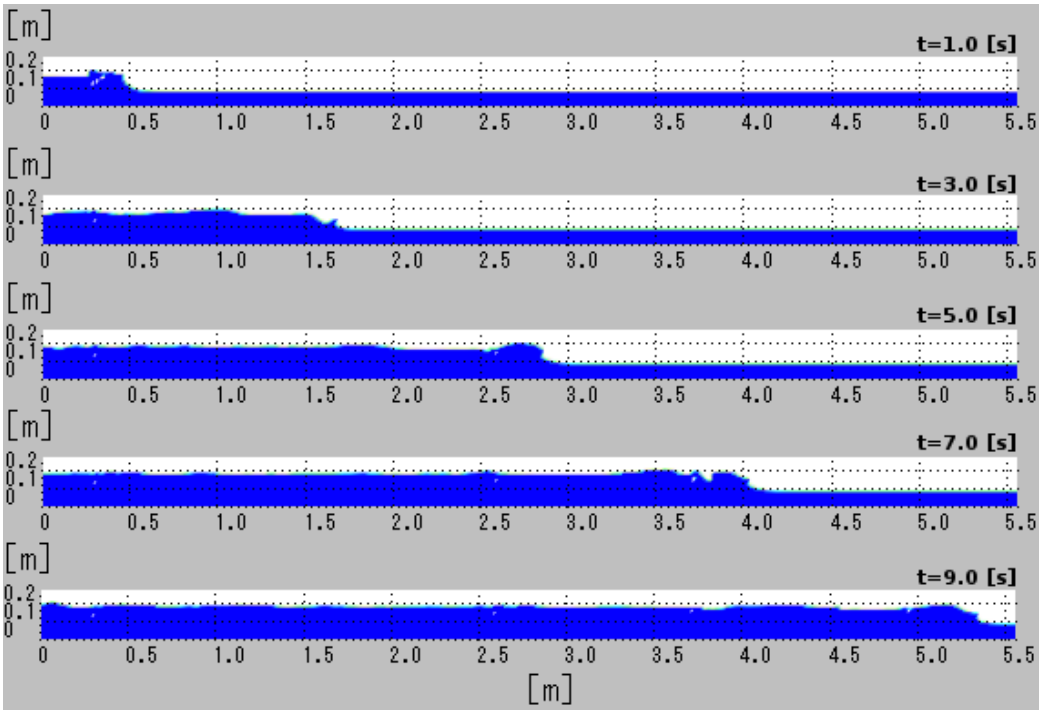

Fig. 8. Free-surface profiles: $t = 1.0$, 3.0, 5.0, 7.0 and 9.0 s.

dimensionless time $t\sqrt{g/d_0}$ beneath a weak surge at $x = 3.90$ m for the Layers 1, 3 and 5 (layers are specified in Table 2).

In Fig. 12, the V_x/V_* values of TCAS model and the data of Koch and Chanson [2009] are compared. In the figure, Layer 1 (black solid line) and 6 (light-gray solid line) were chosen for the comparison with the experiment data of Koch and Chanson [2009] (crosses and squares), and the broken-line shows d/d_0 by the numerical model and triangles shows d/d_0 from experimental data by Koch and Chanson [2009].

4. Discussion

Figure 7 illustrates the generation of a weak positive surge by a rapid partial gate closure, and the conditions are those of Koch and Chanson [2009]. TCAS reproduced the large deformation of the free surface profile at the gate. Figure 8 shows the free surface profile of the tidal bore. The position of the bore front is determined by the rightmost point of the water raise. The celerity of the bore is about 0.588 m/s at $t = 5.0$ s and the bore front position is 2.94 m. In the study of Koch and Chanson [2009], the surge front celerity U was 0.541 m/s. The result of TCAS is in agreement with the experimental result. In the figure, some white spots (i.e. entrained air) are found. The buoyancy effect of the small entrained air is canceled by the the re-initialization method. The influence can be neglected in the work because of the

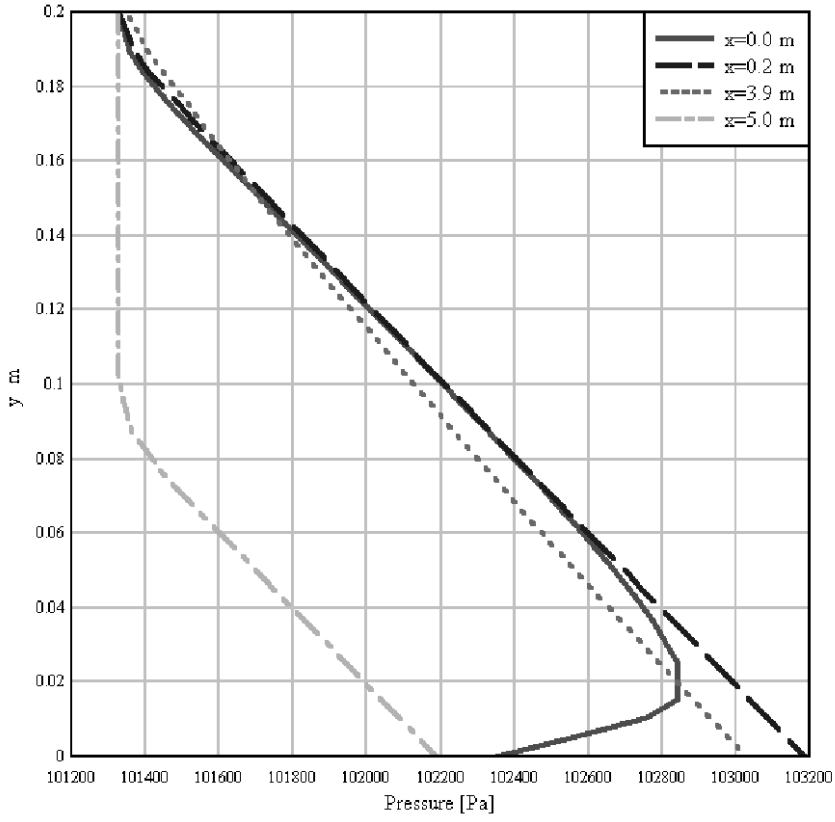

Fig. 9. Vertical pressure profile: $t = 7.0$ s, $x = 0.0$ (solid-line), $x = 0.2$ (broken-line), $x = 3.9$ (dotted-line), $x = 5.0$ (dashed-line) m from the left wall.

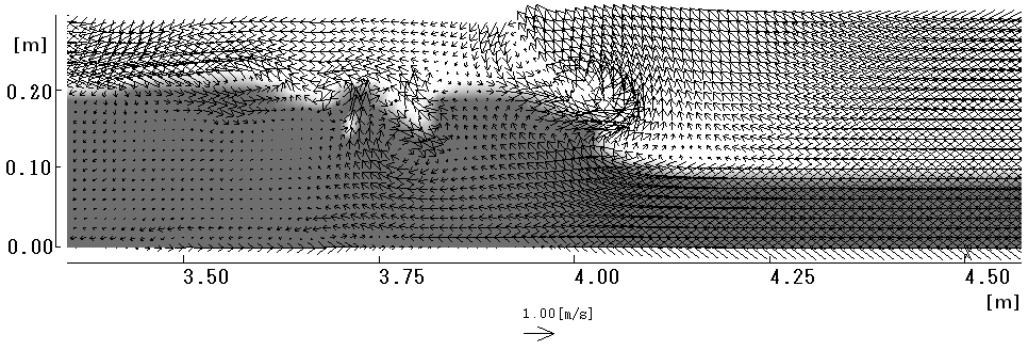

Fig. 10. Velocity profile: $t = 7.0$ s, around $x = 3.9$ m.

large air entrainment is not shown at the tidal bore. However, exact reproduction for the buoyancy effect will be an important task in the future. Figure 9 shows the vertical pressure distribution at $x = 0.0$, 0.2, 3.9 and 5.0 m from the gate. The non-hydrostatic pressure profile is represented at the gate (i.e. $x = 0.0$ m), and the

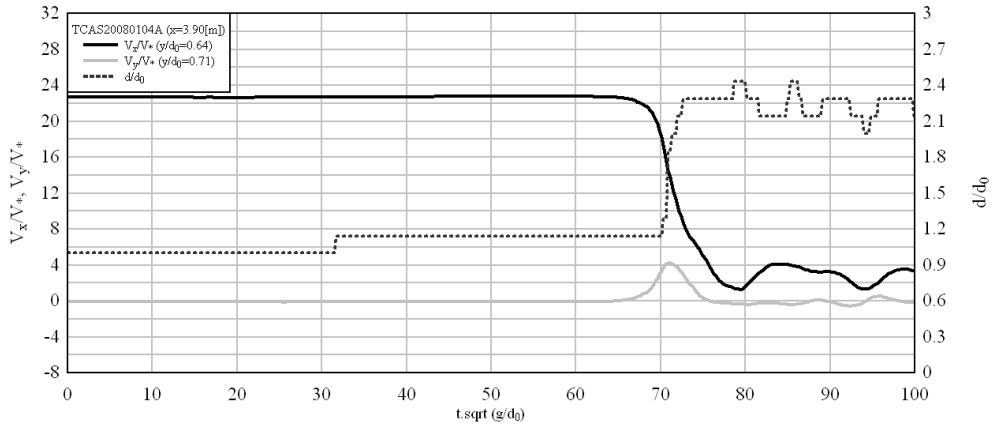

(a)

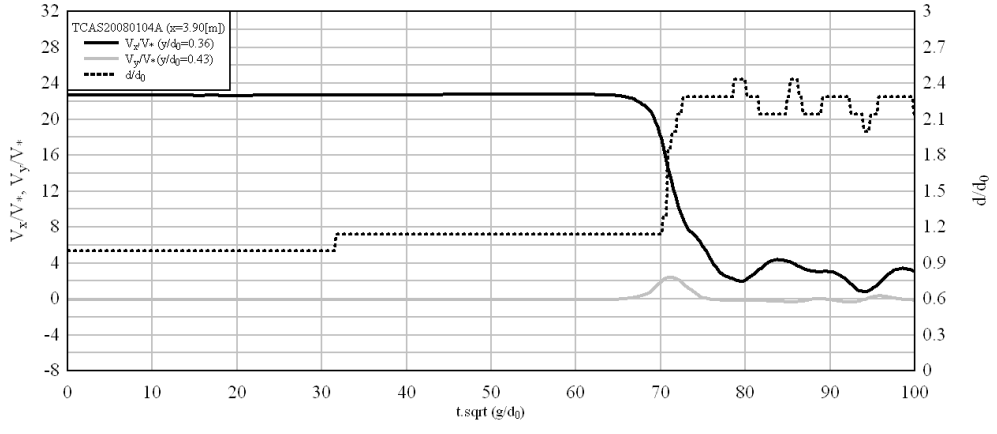

(b)

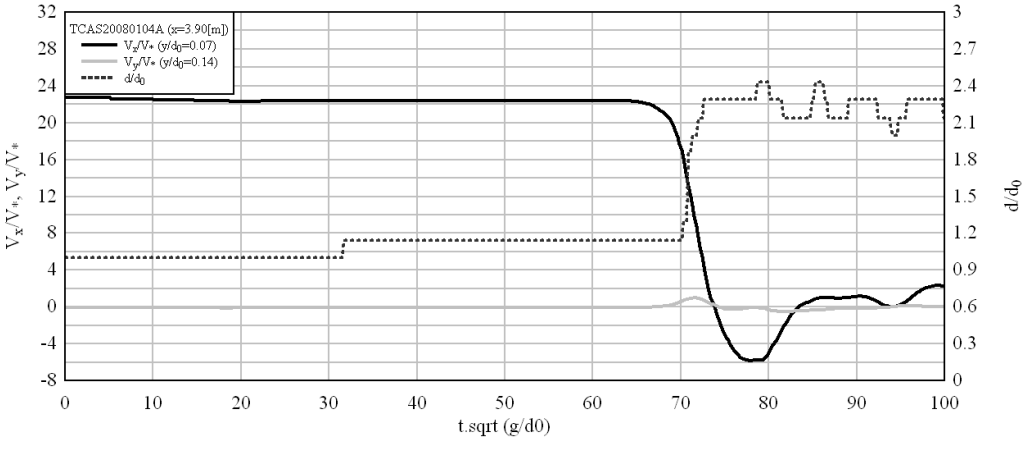

(c)

Fig. 11. Dimensionless instantaneous water depth d/d_0 and velocity components V_x/V_* and V_y/V_* as functions of dimensionless time $t\sqrt{g/d_0}$ beneath a weak surge at $x = 3.90$ m from the gate. Top figure is Layer 5 (near surface layer), middle is Layer 3 and bottom is Layer 1 (bottom layer). (a) Layer 5, (b) Layer 3 and (c) Layer 1.

hydrostatic pressure profile is represented at the other points. It shows the validities of the pressure calculation and the setting of boundary condition at the outlet.

Some flow reversal was observed on the bed (Layer 1 and Layer 2) at 3.4 m $< x <$ 4.0 m in Fig. 10. This is seen in Fig. 11 with some negative instantaneous V_x velocity component data about $t\sqrt{g/d_0} = 77$ in both physical and numerical models (Fig. 11, bottom graph). Next to the free-surface, no such flow reversal was observed (Fig. 11, top graph). The surge front passage was associated with a rapid flow deceleration. Overall the numerical results were in close agreement with the experimental measurements of Koch and Chanson [2009], also presented in Chanson [2009]. (Note the difference in notation. Koch and Chanson [2009] defined V_y as the transverse horizontal velocity component. Herein V_y is the vertical velocity component.) Similarly, the numerical data indicated some relatively large velocity components during the front passage. Koch and Chanson [2009] did not record the vertical velocity component, but their transverse velocity data showed trends that were in agreement with the present numerical investigation.

Figure 12 shows specifically a comparison between numerical and experimental data in terms of the longitudinal velocity component. While the overall trend shows a close agreement between the two approach, it is important to note that

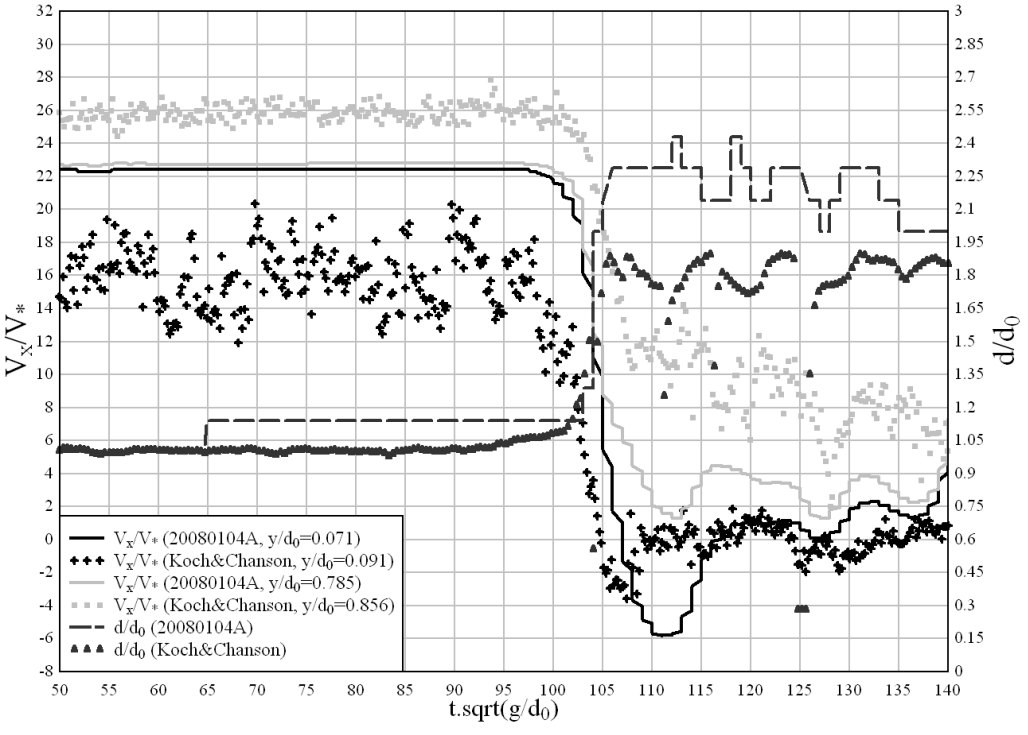

Fig. 12. Dimensionless instantaneous water depth d/d_0 and velocity components V_x/V_* as functions of dimensionless time $t\sqrt{g/d_0}$ beneath a weak surge.

the experimental data provide the instantaneous velocity in a small sampling volume (cylinder of water with a diameter of 4.2 mm and a height of 6.2 mm). In contrast, the numerical results provided a vertical-averaged velocity over the grid element (12 mm high). The vertical depth was modeled with only seven grid elements. Hence, the numerical results did not capture the rapid, fluctuating nature of the instantaneous velocity field nor the details of the turbulent structures. Furuyama and Chanson [2008] considered the numerical validation of TCAS for the dam break flow condition by using several sizes of the grids. The result showed that the mm order size grid was needed for the exact solution. However the sufficiently fine grids are not available because of the enormous calculation time needed. The high speed solver for the pressure and the high speed calculation method e.g. a parallel calculation will be needed for the exact solution.

More, in the TCAS model, a 2nd order finite-difference method was used, but Kajishima *et al.* [1997] showed some improvement of the numerical results using a 4th order finite-difference method. They argued that the 2nd order finite-difference method does not reproduce accurately the high frequency wave components in the GS. In future works, a finer grid size together with a more sophisticated turbulence model may be required to improve the accuracy of the numerical model; e.g. Dynamic Smagorinsky Model (DSM) by Germano *et al.* [1991].

5. Conclusion

In the present study, a numerical model (TCAS) was developed based on the C-CUP method and equipped with a LES model and a re-initialization method. The model was validated with and applied to the tidal bore flow. In the tidal bore with a weak breaking front, the numerical model reproduced accurately the large deformation of the free surface during the bore generation by a downstream gate closure. The free-surface profile and surge front celerity data were in good agreement with the physical data of Koch and Chanson [2005, 2009]. Once the bore was fully-developed, the numerical results showed the existence of some short-lived velocity reversal next to the bed immediately after the bore front passage. This flow feature was documented by Koch and Chanson [2009] and Chanson [2009]. In the future, the numerical model may be applied to a range of civil engineering applications. The C-CUP method has the capability to resolve the interactions between gas, liquid and solid. It can solve accurately free-surface flow situations with large free-surface deformations (e.g. the tidal bore flow). The model could be expanded to scour simulation and sand migration problem, as well as wind-water interaction. The numerical model may be used for disaster prevention, but the effects of calculation resources, including computational memory, computational time, and boundary condition fitting, are important practical issues. Ultimately the introduction of detailed topography data might become the critical element for accurate disaster prevention simulations. Some effective grid generation methods like Adaptive Mesh Refinement (AMR) method might be

effective to decrease the calculation time and improve the accuracy; e.g. Furuyama *et al.* [2006].

Acknowledgments

The authors acknowledge the helpful comments of and discussions with many people, including (in alphabetical order) Professor Shin-ichi Aoki (Toyohashi University of Technology), Professor Colin J. Apelt (The University of Queensland, Australia), Dr Koji Kawasaki (Nagoya University, Japan), and Dr Luke Toombes (Connell Wagner, Brisbane, Australia).

References

Chanson, H. [2007] "Hydraulic jumps: Bubbles and bores," in *Proc. 16th Australasian Fluid Mechanics Conference AFMC*, eds. Jacobs, P., McIntyre, T., Cleary, M., Buttsworth, D., Mee, D., Clements, R., Morgan, R. & Lemckert, C., pp. 39–53, ISBN:978-1-864998-94-8.

Chanson, H. [2009] "Current knowledge in hydraulic jumps and related phenomena. A survey of experimental results," *European Journal of Mechanics B/Fluids* **28**(2), pp. 191–210 (DOI:10.1016/j.euromechflu.2008.06.004) (ISSN:0997-7546).

Eddington, R. B. [1970] "Investigation of supersonic phenomena in a two-phase (liquid-gas) tunnel," *AIAA Journal* **8**(1), 65–74.

Furuyama, S. & Chanson, H. [2008] "A numerical study of open channel flow: Hydrodynamics and turbulence of the tidal bore and dam-break flows," Technical report, Hydraulic Model Report No. CH66/08, Div. of Civil Engineering, The University of Queensland, Brisbane, Australia, 88 pages, ISBN:9781864999068.

Furuyama, S., Hori, T., Tsukurimichi, M. & Aoki, S. [2006] "Realization of highly accurate shore current simulation by using adaptive mesh refinement method," *Annual Journal of Coastal Engineering, JSCE* **53**, 21–25 (in Japanese).

Germano, M., Piomelli, U., Moin, P. & Cabot, W. [1991] "A dynamics subgrid-scale eddy viscosity model," *Phys. Fluids* **A**(3), 1760–1765.

Hirt, C. W. & Nichols, B. D. [1981] "Volume of Fluid (VOF) method for the dynamics of free boundaries," *Journal of Computational Physics* **39**, 201–225.

Hong, C.-B., Doi, Y. & Matsuda, H. [2005] "Numerical study on breaking phenomena of ships' waves in narrow and shallow waterways," *Journal of Marine Science and Technology* **10**, 11–21.

Hornung, H. G., Willert, C. & Turner, S. [1995] "The flow field downsteam of a hydraulic jump," *J. Fluid Mech.* **287**, 299–316.

Kajishima, T. [2003] *Numerical Simulation of Turbulent Flows* (Yokendo Ltd.), ISBN:4-8425-9910-3, (in Japanese).

Kajishima, T., Ohta, T., Oakazaki, K. & Miyake, Y. [1997] "High-order finite-difference method for incompressible flows using collocated grid system," *Transactions of the Japan Society of Mechanical Engineers. B* **63**(614), 3247–3254 (in Japanese).

Kawasaki, K. [2005a] "Numerical model of 2-D multiphase flow with solid-liquid-gas interaction," *International Journal of Offshore and Polar Engineering* **15**(3), 198–203.

Kawasaki, K. [2005b] "Numerical simulation of solid-gas-liquid phase flow in a three-dimensional field," in *Proc. 3rd Int. Conf. Asia and Pacific Coasts*, pp. 1868–1879.

Kawasaki, K. & Hakamata, M. [2006] "Numerical analysis of time-changing wave force acting on drifting rigid structure with solid-gas-liquid phase flow model," in *Proc. 30th Int. Conf. Coastal Engineering*, pp. 4507–4519.

Koch, C. & Chanson, H. [2005] "An experimental study of tidal bores and positive surges: Hydrodynamics and turbulence of the bore front," Technical report, Hydraulic Model Report

No. CH56/05, Div. of Civil Engineering, The University of Queensland, Brisbane, Australia. 170 pages, ISBN:978-1-86499-824-5, 1864998245 [10 digits].

Koch, C. & Chanson, H. [2009] "Turbulence measurements in positive surges and bores," *J. Hyd. Res., IAHR* **47**(1), 29–40, doi:10.3826/jhr.2009.2954.

Lesieur, M., Metais, O. & Comte, P. [2005] *Large-Eddy Simulation of Turbulence* (Cambridge University Press).

Locke, A., Hanson, J. M., Klassen, G. J., Richardson, S. M. & Aube, C. I. [2003] "The damming of the petiticodiac river: Species, populations, and habitats lost," *Northeastern Naturalist* **10**(1), 39–54.

Madsen, P. A., Simonsen, H. J. & Pan, C.-H. [2005] "Numerical simulation of tidal bores and hydraulic jumps," *Coastal Engineering* **52**, 409–433.

Malandain, J. J. [1988] "La seine au temps du mascaret ('The seine river at the time of the mascaret')," *Le Chasse-Marée* **34**, 30–45 (in French).

Mizutani, N., Satoh, Y. & Suzuki, T. [2002] "Development of numerical wind wave tank using scheme to solve gas and liquid mixing flow field — Construction of completely conservation algorithm," Technical report, NILIM. YSK-N-11 (in Japanese).

Momoki, T. & Yoneyama, H. [2005] "Numerical analysis of impulsive breaking wave force that acts on coastal structures by CIP method," in *19th Japan Society of Fluid Mechanics (JSFM) Symposium CD-ROM* (in Japanese).

Nakamura, T., Tanaka, R., Yabe, T. & Takizawa, K. [2001] "Exactly conservative semi-Lagrangian scheme for multi-dimensional hyperbolic equations with directional splitting technique," *Journal of Computational Physics* **174**, 171–207.

Shimizu, F., Tanaka, K., Hatakenaka, K., Shigefuji, H. & Shimizu, T. [2001] "Numerical simulation of gas/liquid interface in water tank using the CCUP scheme," in *15th Japan Society Computational Fluid Dynamics (JSCFD) Symposium CD-ROM* (in Japanese).

Shuto, N. [1985] "The Nihonkai-chubu Earthquake Tsunami on the North Akita Coast," *Coastal Eng. in Japan* **20**, 250–264.

Smagorinsky, J. [1963] "General circulation experiments with the primitive equations," *Mon. Weath. Rev.* **91**(3), 99–164.

Yabe, T., Ishikawa, T., Wang, P. Y., Aoki, T., Kadota, Y. & Ikeda, F. [1991] "A universal solver for hyperbolic equations by cubic-polynomial interpolation," *Computer Physics Communications* **66**, 219–242.

Yabe, T., Takizawa, K., Chino, M., Imai, M. & Chu, C. C. [2005] "Challenge of CIP as a universal solver for solid, liquid and gas," *International Journal for Numerical Method in Fluids* **47**, 655–676.

Yokoi, K. & Xiao, F. [2002] "Mechanism of structure formation in circular hydraulic jumps: Numerical studies of strongly deformed free-surface shallow flow," *Physica D* **161**, 202–219.